Effect of compositional variations on log responses of igneous and metamorphic rocks. II: acid and intermediate rocks

R. PECHNIG[1], H. DELIUS[2] & A. BARTETZKO[1]
[1]*Angewandte Geophysik, RWTH Aachen University of Technology, Lochnerstrasse 4-20, 52056 Aachen, Germany (e-mail: r.pechnig@geophysik.rwth-aachen.de)*
[2]*Department of Geology, University of Leicester, Leicester, LE1 7RH, UK*

Abstract: An extensive data-set of petrophysical down-hole measurements exists for boreholes drilled into continental crystalline crust. We selected boreholes covering a range of different types of plutonic rocks and gneisses in amphibolite or high-grade metamorphic rocks. According to Serra's concept of electrofacies, a specific set of log responses should characterize one rock type. Here, we concentrate on the detection of compositional variations between rock types. Bulk composition of the protoliths influences the mineralogical composition of the metamorphic rock, and we demonstrate how this impacts on the down-hole measurements. Integration of logging data with geochemical core data and mineralogical descriptions allows the calibration of the log responses to rock types. The relationship of the log responses with core data shows a remarkably good correlation, and diagnostic trends are detected. From the logs, potassium and neutron porosity are particularly helpful in distinguishing different types of gneisses and igneous rocks with respect to their protoliths. The proportions of amphibole/pyroxene, mica + K-feldspar and feldspar + quartz in the rocks seem to control the direction of correlation in a cross-plot, i.e. positive or negative, depending on increasing or decreasing mineral proportions. This is true for all boreholes, and a generalized classification scheme could be developed for these crystalline rocks.

Introduction

During the last few decades, several boreholes were drilled into igneous and metamorphic basement rocks. Exploration drilling has been performed for the purposes of mineral mining, tapping geothermal energy or disposal of wastes as well as in the framework of research drilling in continental or oceanic crust. In contrast to well logging in the traditional hydrocarbon environment, information about log responses in igneous and metamorphic rocks is scarce. This is especially true for the acid and intermediate rocks of the continental basement. Besides some early compilations of log responses from the principal igneous and metamorphic rocks (Keys 1979; Desbrandes 1982), most studies performed hitherto have focused on single boreholes drilled into continental basement (Daniels *et al.* 1983; Sattel 1986; Paillet 1991; Pratson *et al.* 1992; Traineau *et al.* 1992; Nelson & Johnston 1994; Pechnig *et al.* 1997). These studies showed that the complex geological conditions of crystalline rocks, particularly metamorphic rocks, are not easily determined from the logs, because of the superposition of log responses produced by the varying compositional and structural variations of crystalline rocks. Hitherto, no systematic interpretation or classification charts are available for crystalline rocks. Therefore, this study is focused on a comparison of igneous and metamorphic rock types from drill-holes in continental basement. It comprises, besides foregoing electrofacies analyses individually performed for the different holes, a core log integration to develop classification charts, which include all available information on rock chemistry and mineralogy.

Log and lithological data compilation

This study is based on a comparison of wireline data with mineralogical and geochemical data from core and cuttings samples. Log, core, and cuttings data from the following boreholes were compiled and analysed: KTB pilot hole, Leuggern, Schafisheim, Böttstein, Soultz-sous-Forêts GPK1, Moodus and Cajon Pass (Fig. 1). These boreholes cover a wide range of different

From: HARVEY, P. K., BREWER, T. S., PEZARD, P. A. & PETROV, V. A. (eds) 2005. *Petrophysical Properties of Crystalline Rocks*. Geological Society, London, Special Publications, **240**, 279–300.
0305-8719/05/$15.00

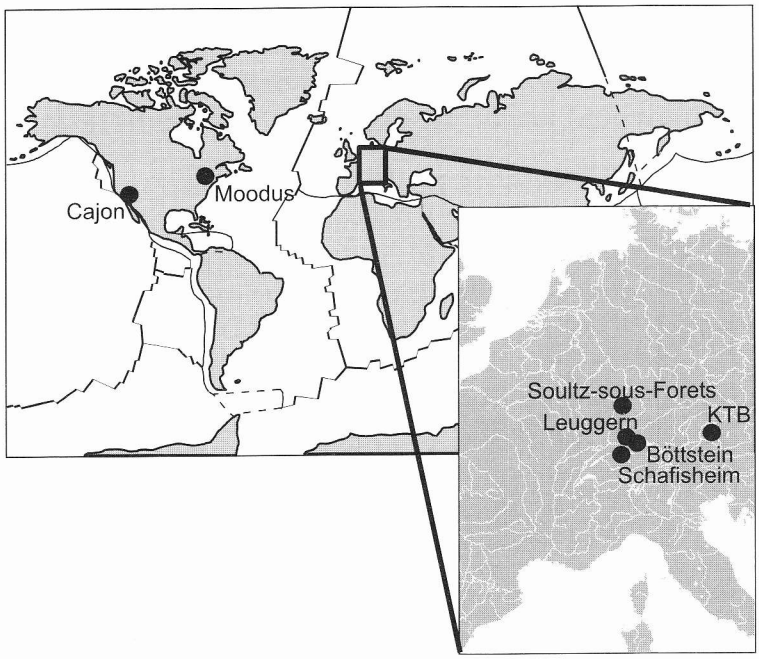

Fig. 1. Location of the boreholes compared in this study.

types of acid to intermediate plutonics, orthogneisses and paragneisses. From each borehole, one or several intervals were chosen to be representative for the lithology. Intervals were selected using the following criteria:

(1) general availability and quality of the logging data;
(2) availability of core/cuttings information;
(3) intervals with good borehole conditions to avoid logging tool failure sources from borehole enlargements, and
(4) homogeneous sequences and large bed thickness, to minimize log integration effects on bed boundaries. Since the focus of this study is concerned with the effect of the rock composition on the tool responses, fractured, brecciated and strongly altered intervals were generally excluded.

Geological setting and lithology of the selected boreholes

Metamorphic rocks were drilled in the boreholes KTB (Emmermann & Lauterjung 1997; Hirschmann *et al.* 1997), Moodus (Naumhoff 1988), Leuggern (Peters *et al.* 1989*a*) and Cajon Pass (Silver *et al.* 1988). The rocks drilled in these boreholes mainly comprise paragneisses, orthogneisses and metabasites overprinted by amphibolite-facies up to granulite-facies metamorphism. Plutonic rocks were drilled in the boreholes Soultz-sous-Fôrets (Traineau *et al.* 1992), Böttstein (Peters *et al.* 1986) and Schafisheim (Matter *et al.* 1988), and in the deeper parts of the Leuggern borehole (Peters *et al.* 1989*a*). The drilled rocks include granites to granodiorites, syenites and monzonites. An overview of the boreholes, their rock content and petrogenetic evolution is given in Table 1 and Figure 2, and is summarized in the following section.

The German Deep Continental Drilling Project KTB drilled two deep holes at the western margin of the Bohemian Massif. The drill site itself lies within the Zone of Erbendorf–Vohenstrauss (ZEV), a small crustal segment of the Variscan orogenic belt. Two boreholes, separated by only a short distance of 200 m from each other, were drilled. The pilot hole (KTB-VB) reached a final depth of 4001 m, and was almost completely cored. The drilled crustal segment consists of an alternating sequence of three main lithological units: paragneisses, metabasites and 'variegated' units of paragneiss–metabasite alternations (Emmermann & Lauterjung 1997). All these units have suffered pervasive metamorphism to

Table 1. *Overview of general borehole data, lithology and petrogenetic evolution*

Borehole	Total depth (m)	Core recovery in basement (%)	Selected depth intervals (m)	Rock content of the selected intervals	Igneous and metamorphic evolution
Schafisheim	2006	90	1495–1560, 1600–1680 1710–1730, 1760–1960	Biotite-granite, monzonite, syenite, aplite	316 Ma: crystallization age of rocks 300–230 Ma: 1. Pervasive hydrothermal stage 280–260 Ma: 2. tectono-hydrothermal overprint
Böttstein	1501	75	595–800	Biotite-granite	330–320: granite intrusion 300–230 Ma: 1. pervasive hydrothermal stage 280–260 Ma: 2. tectono-hydrothermal overprint
Leuggern	1690	98	300–500, 720–750, 770–850, 960–1200, 1450–1600	Biotite-granite, sillimanite-bearing biotite-paragneiss, hornblende gneiss	500 Ma: 1. amphibolite-facies overprint during Caledonian orogeny 380 Ma: 2. amphibolite-facies overprint 330–320 Ma: granite intrusions followed by 1. hydrothermal overprint and cataclastic deformation of gneisses 280–260 Ma: 2. hydrothermal overprint
Soultz GPK1	2000	7	1450–1990	Biotite-granite	316 ± 7 Ma: granite intrusion and following 1. hydrothermal stage during cooling of the batholith 280–260 Ma: 2. tectono-hydrothermal overprint
Cajon Pass	3550	<3	2650–3100	Acid to mafic orthogneisses	81–75 Ma: amphibolite-facies overprint (T 600–750°C; *P* 3–6 kbar)
Moodus	1460	<2	200–400, 580–625, 825–955, 1100–1200	Biotite-paragneisses, acid orthogneisses, hornblende gneiss	390 Ma: amphibolite-facies overprint
KTB-VB	4000	93	570–900, 2500–2650, 3410–3440	Biotite-paragneisses, hornblende gneisses	375–405 Ma: higher amphibolite-facies overprint

References for petrogenetic data: Leuggern, Böttstein and Schafisheim: Thury *et al.* (1994), Soultz GPK1: Chevremont & Genter (1988), Cajon Pass: (3) Silver *et al.* (1988); Moodus: Wintsch & Aleinikoff (1987); and KTB-VB: O'Brien *et al.* (1997).

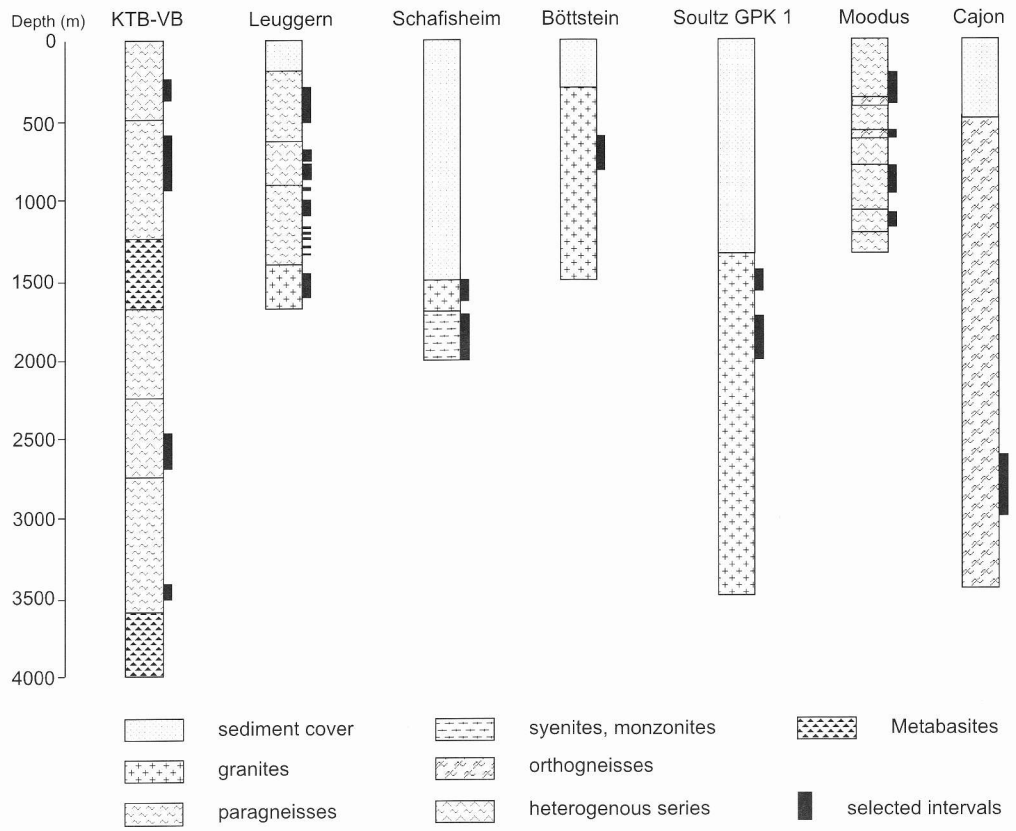

Fig. 2. Schematic lithological overview of the boreholes and the intervals selected for this study.

upper amphibolite facies, dated at between 405 and 375 Ma ago (O'Brien *et al.* 1997). The whole section is characterized by steeply dipping foliation (50–70°) and abundant fault zones resulting from multi-stage brittle deformation (Hirschmann *et al.* 1997).

As part of an extensive Swiss research programme focused on the evaluation of possible radioactive waste repositories, seven deep boreholes were drilled in northern Switzerland. Three of these boreholes were selected for this study: Leuggern, Schafisheim and Böttstein. The boreholes reached final depths between 1300 and 2500 m. In total, about 3000 m were drilled through crystalline rocks, most of it completely cored and thus extremely well documented. The boreholes revealed the crystalline basement as a complex mixture of metamorphic and igneous rocks. The metamorphic units are mainly composed of metasediments with minor intercalations of mafic rocks (Peters *et al.* 1986, 1989*a*, 1989*b*). These rocks underwent high-grade amphibolite-facies to granulite-facies conditions about 500 Ma ago, followed by different stages of ductile deformation (Thury *et al.* 1994). During the final stage of the Variscan orogeny (330–315 Ma) large volumes of granitic melt were intruded into the gneiss series. The intrusions were accompanied by strong cataclastic deformation and hydrothermal overprinting of the metamorphic series. A later tectonohydrothermal event during the Lower Permian strongly altered the granites (Thury *et al.* 1994).

The borehole GPK1 is located on the western side of the Rhine Graben near Soultz-sous-Forêts (France), in a region with an unusually high geothermal gradient. The well was drilled as part of the Franco-German 'Hot Dry Rock' project, in order to test the feasibility of establishing a deep geothermal heat exchanger. GPK1 was drilled in 1988, reaching a depth of 2000 m, through 1376 m of sedimentary cover into the underlying granite. Only a few cores, with a total length of 43 m, were taken. The granites crystallized about 316 $\pm$ 7 Ma ago (Chevremont & Genter 1988). The massif is

mainly composed of porphyroid granite with intercalated fine-grained leucogranitic intrusions, both affected by pervasive alteration. Hydrothermally altered zones of several metres in thickness are frequently observed along major fracture zones, where the granite is significantly altered (Genter 1989; Genter *et al.* 1989; Traineau *et al.* 1992).

The Moodus borehole extends to a depth of 1460 m near the town of Moodus in central Connecticut, USA. In 1987 the well was drilled into the crystalline rocks of the eastern Appalachians, with the objective of evaluating seismic hazard risks for the installation of power plants. Nine cores, roughly 2.5 m in length, were recovered at 150 m intervals, and cuttings were collected at 6 m intervals (Naumhoff 1988). The drilled lithology consists of paragneisses and orthogneisses of acid to intermediate composition, with minor intercalations of mafic metamorphic rocks. Two different terranes of the Appalachian mountain belt were encountered. In the upper part, the hole penetrates rocks of the Early Palaeozoic Merrimack terrane, and passes at about 820 m into the underlying Avalon terrane (Naumhoff 1988). Based on radiometric age determinations, these rocks are Late Precambrian in age (620 Ma; Wintsch & Aleinikoff 1987). The Merrimack and the Avalon terranes are separated by a major ductile thrust fault system called the Honey Hill fault zone. Mineral assemblages associated with the fault zone indicate that the dominant ductile fabric developed under amphibolite-grade metamorphic conditions about 390 Ma ago (Naumhoff 1988). In contrast to the other boreholes described, the rocks drilled in the Moodus borehole only locally show a greenschist-facies overprint, and brittle deformation is rare.

The Cajon Pass scientific borehole, 4 km north of the San Andreas Fault in California, was drilled to measure the heat flow and state-of-stress at seismogenic depth to explain the 'heat-flow-stress paradox' observed in the San Andreas fault zone (Lachenbruch and Sass 1988). The borehole was drilled to 3.55 km into a series of plutonic rocks and orthogneisses. Information on lithology is mostly based on cuttings, since only 3% of the borehole was cored. The rocks are orthogneisses of gabbroic to granitic composition, and were overprinted under amphibolite-facies conditions 75–81 Ma ago almost sychronously with dioritic intrusions (Silver *et al.* 1988). A Late Miocene tectonic phase resulted in the formation of 'low angle fractures', which, during the Pliocene, acted as pathways for hydrothermal fluid circulation and corresponding zeolite-facies alteration (Vincent and Ehlig 1988).

Mineralogical and geochemical composition of the rocks

Geochemical data-sets and information on rock modal composition were collected from the literature (Matter *et al.* 1988; Peters *et al.* 1989*a*, *b*; Peters *et al.* 1986; Genter *et al.* 1989; Silver *et al.* 1988; Ambers 1989; KTB-Data CD). The rock modal data comprise results from point counting and X-ray diffraction analyses. The average geochemical and mineralogical compositions for 25 rock types are displayed in Tables 2 & 3. The bulk composition of the rocks can be summarized as follows.

The biotite granites and aplites of the boreholes: Schafisheim, Leuggern, Böttstein and Soultz-sous Forêts GPK1 show comparable granitic chemical signatures, with tendencies towards alkaline composition for the Schafisheim granite and aplite (Fig. 3). The main chemical differences concern the K_2O content, which corresponds to variations in the average potassium-feldspar volume between 17% and 41%. The variations in K-feldspar contents are caused by the substitution of K-feldspar by plagioclase, while quartz and biotite proportions remain almost constant in the granites. Compared to the granites, the aplites have lower biotite contents.

The monzonites and syenites of the Schafisheim borehole were classified after Streckeisen with regard to their modal composition (Matter *et al.* 1988). Low quartz contents and high amphibole contents separate them from the other plutonic rocks compiled for this study. Although the monzonites and syenites show considerable differences in their modal composition, their average chemical composition is quite similar, both plotting into the syeno-diorite field (Fig. 3). Larger differences between syenites and monzonites concern the potassium and sodium concentrations controlling the varying potassium-feldspar/plagioclase ratio of these rocks (Table 3).

The rocks of the orthogneiss group span a suite from almost gabbroic composition to leucocratic gneisses of granitic composition. Their chemical signature is widely controlled by the stage of magmatic differentiation of the plutonic precursor rocks as visible for the Cajon Pass orthogneisses (Fig. 3). The average element contents and modal composition of the Cajon granitic gneiss are in the range of the biotite granites from the other boreholes. Higher quartz contents are documented for the Moodus granitic gneiss. This observation is in agreement with the higher SiO_2 values measured in this rock type.

Table 2. *Rock mineralogical composition compiled from petrographic and XRD analyses*

Lithology	Hole	*n*	Quartz		K-feldspar		Plagioclase		Biotite		Muscovite		Chlorite (sillimanite)		Garnet (cordierite)		Amphibole (pyroxene)		Ref.
			Range	Mean	Range	Mean	Range	Mean	Range	Mean	Range	Mean	Range	Mean	Range	Mean	Range	Mean	
								Plutonic rocks											
Biotite granite	Schaf.	22	15–32	23	27–53	41	10–30	22	2–14	9	—	—	—	—	—	—	—	—	(1)
	Leug.	10	15–30	23	25–45	35	20–40	31	5–15	11	—	—	—	—	(<4)	(1)	—	—	(2)
	Bött.	12	15–33	27	30–45	38	20–40	28	5–15	8	—	—	—	—	(<4)	(1)	—	—	(3)
	GPK1	3	20–38	28	15–27	19	35–45	40	<10	8	—	—	—	—	—	—	—	—	(4)
Monzonite	Schaf.	8	1–15	3	16–37	28	16–34	25	11–27	21	—	—	—	—	—	—	20–32	23	(1)
Syenite	Schaf.	21	0–5	2	20–50	39	3–13	7	13–33	26	—	—	—	—	—	—	13–33	23	(1)
Aplite	Schaf.	5	25–30	28	16–35	27	26–43	34	2–10	5	—	—	—	—	—	—	—	—	(1)
	Leug.	9	34–40	38	8–35	17	25–50	35	<5	2	0–10	5	—	—	—	—	—	—	(2)
								Orthogneisses											
Gabbroic	Cajon	*	NA	—	NA	—	NA	42	NA	4	NA	—	NA	—	NA	—	NA	50	(5)
Dioritic	Cajon	*	NA	20	NA	—	NA	55	NA	20	NA	—	NA	—	NA	—	NA	5	(5)
Granodioritic	Cajon	*	NA	21	NA	16	NA	50	NA	7	NA	—	NA	—	NA	—	NA	5	(5)
Granitic	Cajon	*	NA	29	NA	41	NA	23	NA	7	NA	—	NA	—	NA	—	NA	—	(5)
	Mood.	3	30–35	34	30–32	31	31–33	32	1–5	3	<1	0	—	—	—	—	—	—	(6)
K-feldspar	Mood.	1	30	30	35	35	35	35	—	—	—	—	—	—	—	—	—	—	(6)
Quartz–feldspar	Mood.	3	30–33	32	34–35	34	30–35	34		—	—	—	—	—	—	—	—	—	(6)
								Paragneisses											
(Sillimanite)–biotite	Leug. a	†	30–50	40	<8	4	25–45	35	15–45	28	<3	1	—	—	<5	2	—	—	(2)
	Leug. b	†	15–30	23	—	—	25–45	35	25–35	30	5–30	17	(10–20)	(15)	<10	5	—	—	(2)
	Leug. c	†	15–40	28	0–35	18	10–25	18	0–30	15	—	—	(0–10)	(5)	(15–50)	(32)	—	—	(2)
	KTB	393‡	25–55	40	—	—	15–35	26	0–25	6	3–28	15	5–30	12	<5	—	—	—	(7)
	Mood.	9	30–40	34	—	—	32–43	36	20–25	23	<10	2	—	—	—	—	(<10)	(3)	(6)
Hornblende	Leug.	†	15–40	28	<30	15	25–40	33	10–20	15	—	—	—	—	—	—	5–30	17	(1)
	KTB	72‡	15–35	24	0–15	5	24–48	33	0–15	3	<10	1	0–17	7	0–7	1	7–34	18	(7)
	Mood.	11	30–40	36	—	—	38–52	43	5–20	11	—	—	—	—	—	—	0–20	9	(6)
K-feldspar	KTB	16	9–21	12	12–37	22	20–50	44	0–18	5	—	—	0–18	10	<2	0	0–12	5	(7)
Quartz–plag.	KTB	12	30–40	35	0–7	1	42–60	52	0–10	3	0–14	5	0–11	5	—	—	—	—	(7)

References (1) Matter *et al.* (1988); (2) Peters *et al.* (1989); (3) Peters *et al.* (1986); (4) Genter *et al.* (1989); (5) Silver *et al.* (1988); (6) Ambers (1989); and (7) KTB-Data CD.
Leug. a: plagioclase–biotite gneiss (metagreywacke); Leug. b: sillimanite–biotite gneiss (metapelite); Leug. c: cordierite–sillimanite gneiss (migmatic metapelite).
*Typical modes of the main rock types of the Cajon Pass borehole are extracted from a total of 120 rock samples.
†Typical value ranges of the Leuggern gneisses summarized from modal analyses; number of analyses is not given.
‡Values combine petrographic and RDA analyses.
NA: Information is not available.

Table 3. *Mean major-element values of the selected rocks*

Lithology	Hole	*n*	SiO_2	Al_2O_3	K_2O	Na_2O	CaO	Fe_2O_3	FeO	MgO	TiO_2	Ref.
						Plutonic rocks						
Biotite granite	Schaf.	8	69.0	13.9	5.7	3.4	1.6	9.2	0.8	1.2	0.5	(1)
	Leug.	10	69.1	14.7	5.2	2.9	1.5	0.4	2.1	1.3	0.5	(2)
	Bött.	12	71.1	14.3	4.9	2.7	1.4	0.5	1.6	0.9	0.4	(3)
	GPK1	3	66.8	14.2	4.1	3.9	2.2	4.3		1.5	0.7	(4)
Monzonite	Schaf.	8	50.1	14.3	5.1	2.7	5.7	1.8	5.9	7.7	1.5	(1)
Syenite	Schaf.	19	49.3	12.5	6.2	1.5	6.1	1.8	5.9	10.1	1.5	(1)
Aplite	Schaf.	7	69.7	14.3	4.6	4.5	1.5	0.7	1.1	0.7	0.3	(1)
	Leug.	13	74.1	13.6	4.3	3.4	0.9	0.5	0.6	0.4	0.1	(2)
						Orthogneisses						
Gabbroic	Cajon	1	53.8	14.8	1.7	2.9	7.7		9.5	5.1	1.0	(5)
Dioritic	Cajon	5	60.3	16.9	2.6	4.1	5.3		5.3	2.6	0.8	(5)
Granodioritic	Cajon	6	61.5	15.7	3.4	3.5	5.1		5.2	3.0	0.7	(5)
Granitic	Cajon	1	71.1	14.0	4.3	3.4	2.0		1.4	0.5	0.2	(5)
	Mood.	*298	77.6	13.8	5.4	NA	2.3	0.5		0.1	0.1	
K-feldspar	Mood.	*577	73.5	12.9	4.5	NA	3.7	3.0		1.6	0.5	
Quartz–feldspar	Mood.	*586	74.4	12.4	4.8	NA	2.0	1.6		4.6	0.3	
						Paragneisses						
(Sillimanite)–biotite	Leug. a	10	74.2	12.0	2.4	2.6	1.4	0.8	2.4	1.2	0.5	(2)
	Leug. b	18	60.3	19.5	4.2	0.9	2.5	1.6	4.7	1.9	0.8	(2)
	KTB	32	64.4	15.8	2.6	2.7	1.3	6.0		2.4	0.9	(6,7)
	Mood.	*2541	70.8	12.3	3.4	NA	4.8	4.7		2.7	0.8	
Hornblende	Leug.	3	60.3	14.7	2.4	3.5	3.5	3.2	4.8	3.5	1.4	(1)
	KTB	7	56.0	15.0	2.0	2.9	5.2	8.3		3.8	1.3	(6,8,9)
	Mood.	*2707	68.3	14.0	2.7	NA	5.2	3.5		5.6	0.6	
K-feldpar	KTB	8	52.4	15.5	3.3	3.7	5.2	8.6		3.1	1.1	(6,8)
Quartz–plag.	KTB	2	66.8	16.0	1.7	4.9	2.1	3.9		2.7	0.5	(6,10)

References (1) Matter *et al.* (1988); (2) Peters *et al.* (1989*b*); (3) Peters *et al.* (1986); (4) Traineau *et al.* (1992); (5) Silver *et al.* (1988); (6) KTB-Data CD; (7) Heinschild *et al.* (1988); (8) Stroh & Tapfer (1988); (9) Tapfer *et al.* (1989); Wittenbecher *et al.* (1989).
Leug. a: plagioclase-biotite gneiss (metagreywacke).
Leug. b: cordierite-bearing sillimanite–biotite gneiss (metapelite).
*Mean values calculated from geochemical logging data.
NA: Information is not available.

Compared to the selected plutonic rocks and orthogneisses, the paragneisses show a more complex mineralogical composition. Besides the main components (quartz, feldspar, biotite and amphibole in varying amounts), white mica, sillimanite, cordierite and garnet also occur. The present mineralogical composition is mainly caused by the original sediment bulk composition, but is also affected by the degree of metamorphism. The biotite gneisses show strong variations in quartz content (15–55%) and the amount of biotite, white mica and sillimanite (Hirschmann *et al.* 1997; Naumhoff 1988; Peters *et al.* 1989*a*). Besides the migmatitic version of the Leuggern paragneisses, all other types contain almost no K-feldspar. Pyroxene is observed only in the Moodus biotite gneisses. The chemical composition of the biotite gneisses of the different boreholes varies significantly, corresponding with changes in the modal composition.

Hornblende paragneisses were drilled in the boreholes Leuggern, KTB and Moodus. The precursor rocks are siliciclastic sediments mixed with mafic rock components of volcanic origin, such as ashes or volcaniclastics (Harms *et al.* 1997; Hirschmann *et al.* 1997; Naumhoff 1988; Peters *et al.* 1989*a*). The relative proportions of siliciclastics and volcanic components determine the overall chemistry and mineralogy of the hornblende gneisses. Thus, they show considerable differences in their mean mineralogical composition, particularly regarding the quartz, amphibole and biotite contents.

Petrophysical characteristics of the rocks

A wide spectrum of logging operations were carried out in the selected boreholes, including the recording of acoustic, electric and nuclear data. The logs that were evaluated for this study (Table 4) were performed by the following Schlumberger tools: the dual laterolog (DLL); litho density tool (LDT); natural gamma-ray spectroscopy tool (NGT); compensated neutron

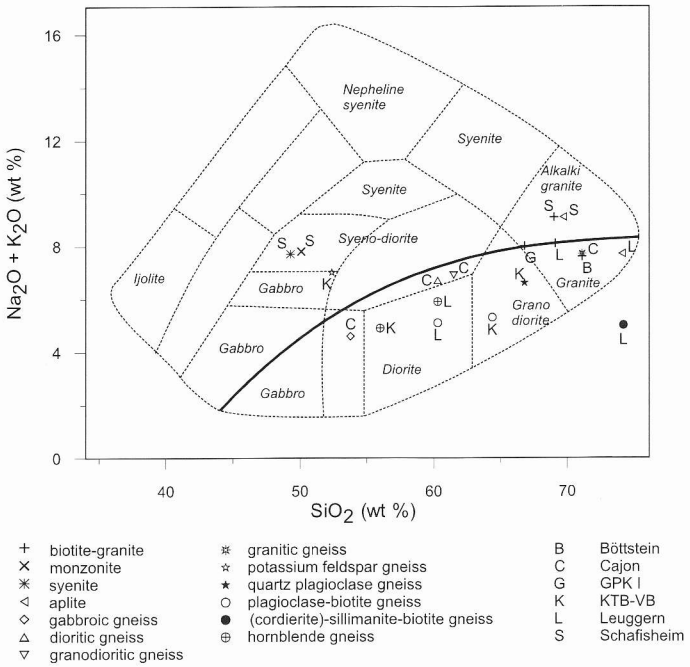

Fig. 3. Total alkali versus silica diagram for the chemical analyses of rock types selected for this study (modified after Wilson 1989).

tool (CNT); and different sonic tools, such as the digital sonic array tool (DST) and the compensated sonic tool (CST). General information on logging tools and their measurement principles can be found in Ellis (1987), Rider (1996) and Hearst & Nelson (2000).

Log analysis was carried out by applying the electrofacies method, originally introduced by Serra (1984) for log interpretation in sedimentary rocks. Like a lithofacies description, which comprises several petrographic and chemical characteristics, the electrofacies method combines the petrophysical value ranges recorded by different logging tools. An electrofacies characterizes a rock type by a specific set of log responses, and thus allows it to be distinguished from others. The concept is not restricted to the use of electrical measurements. Any log property suitable for the characterization of a rock type may be used. This study incorporates the log curves for total gamma-ray, potassium, bulk density, neutron porosity, electrical resis-

Table 4. *Overview of tools and logs used for this study*

Tool	Log		Principle
DLL (dual laterolog)	LLD (ohm m)	Laterolog deep	Electrical resistivity
SDT (Sonic digital tool)	DTCO ($\mu s\ m^{-1}$)	Compressional-wave travel time	Travel time of sound
DSI (Dipole shear sonic imager)			
CNT (compensated neutron tool)	NPHI (%)	Neutron porosity	Absorption of neutrons
LDT (litho density tool)	RHOB ($g\ cm^{-3}$)	Bulk density	Absorption/scattering of gamma-rays
NGT (natural gamma spectrometry tool)	SGR (API*)	Spectral (total) gamma-ray	Natural gamma-ray emissions
	POTA (%)	Potassium content	
	THOR (ppm)	Thorium content	
	URAN (ppm)	Uranium content	

*API: American Petroleum Institute.

tivity and P-wave velocity as being standard logging parameters.

Log analysis was carried out separately for each borehole. All available information on core and cuttings descriptions was collected and, using core–log-correlation, the *in situ* logging data were assigned to the different magmatic and metamorphic rock types. A total of 25 electrofacies were defined. Tables 5–7 display the log value statistics for the rock types separated within the different boreholes. The minimum, maximum, mean values and standard deviation are given for each electrofacie. The data are calculated from the borehole sections marked in Figure 2, taking into account the selection criteria defined on p. 280. Figure 4 displays these values graphically. The similarities and differences in the borehole geophysical characteristics can be summarized as follows.

The gamma-ray values cover a large value range (40–550 API) within the plutonic rocks and gneisses. The average gamma-ray values of the plutonic rocks are about 250 API for the granites/aplites and about 350 API for the syenites/monzonites, and are thus significantly higher than the gamma-ray mean values of all the gneisses. Highest values occur in the Schafisheim monzonites, with about 550 API. Besides the granitic gneiss and the K-feldspar gneiss of the Moodus borehole, all of the other gneisses have lower gamma-ray values (<210 API) than the igneous rocks. The potassium log responses in general correlate with the gamma-ray ones, showing on average higher potassium contents for the plutonic rocks than for the gneisses.

The investigated rocks have bulk density values from 2.30 g cm^{-3} to 2.95 g cm^{-3} with strong variation within the three groups of plutonics, ortho- and paragneisses. The average bulk density of granites and aplites ranges between 2.59 ± 0.02 g cm^{-3} and 2.65 ± 0.02 g cm^{-3}, which is in excellent agreement

Table 5. *Electrofacies statistics displayed for the different rock types. Minimum, maximum mean, and standard deviation of gamma-ray and potassium log responses*

Lithology	Hole	Total gamma ray (API)					Potassium (%)				
		Min	Max	Mean	SD	*n*	Min	Max	Mean	SD	*n*
					Plutonic rocks						
Biotite	Schafisheim	187	356	259	32	462	3.55	5.82	4.79	0.40	462
Granite	Leuggern	163	312	257	17	984	4.31	6.92	5.85	0.38	984
	Böttstein	181	304	230	19	662	4.37	6.59	5.35	0.40	662
	GPK1	196	308	260	18	1005	3.73	7.93	4.96	0.50	1005
Leucogranite	GPK1	130	280	225	35	320	3.87	6.36	5.30	0.50	320
Monzonite	Schafisheim	127	548	333	64	456	4.31	8.91	6.30	0.90	456
Syenite	Schafisheim	215	510	332	58	532	4.47	8.44	6.84	0.74	532
Aplite	Schafisheim	168	329	244	33	242	4.06	6.62	5.29	0.39	242
	Leuggern	157	333	252	32	406	3.58	6.79	5.57	0.59	406
					Orthogneisses						
Gabbroic	Cajon	44	100	73	11	61	1.73	2.51	1.95	0.18	61
Granodioritic	Cajon	66	210	97	20	720	2.36	4.07	3.21	0.28	720
Dioritic	Cajon	59	198	91	16	1028	2.03	3.57	2.68	0.21	1028
Granitic	Cajon	80	165	106	15	343	3.35	4.52	4.03	0.28	343
	Moodus	156	433	202	31	298	3.43	7.99	4.57	0.65	298
K-feldspar	Moodus	111	363	176	45	448	2.57	5.75	3.62	0.55	448
Quartz–feldsp.	Moodus	64	134	109	12	264	1.77	5.31	4.05	0.78	264
					Paragneisses						
(Sillimanite)	Leuggern*	82	192	141	16	903	2.33	5.76	3.90	0.54	903
Biotite gneiss	Leuggern†	90	211	151	19	1546	1.99	6.14	4.32	0.61	1546
	KTB-VB	72	136	99	11	1856	1.44	3.34	2.39	0.38	1856
	Moodus	98	167	121	10	755	2.06	4.22	2.91	0.33	755
Hornblende gneiss	Leuggern	75	169	133	22	130	1.50	4.04	2.53	0.63	130
	KTB-VB	53	99	77	8	664	1.33	2.57	1.88	0.23	664
	Moodus	35	135	81	16	1116	1.17	3.91	2.34	0.46	1116
K-feldspar	KTB-VB	79	185	138	26	101	1.83	5.62	3.85	1.02	101
Quartz–plag.	KTB-VB	66	100	76	7	109	1.35	2.46	1.8	0.05	109

*Plagioclase–biotite gneiss (metagreywacke).
†Cordierite-bearing sillimanite–biotite gneiss (metapelite).
SD: standard deviation.

Table 6. *Electrofacies statistics displayed for the different rock types. Minimum, maximum mean, and standard deviation of density and neutron log responses.*

	Hole	Density (g cm^{-3})					Neutron porosity (%)				
		Min	Max	Mean	SD	*n*	Min	Max	Mean	SD	*n*
					Plutonic rocks						
Biotite	Schafisheim	2.55	2.64	2.61	0.02	462	0.6	4.0	1.7	0.6	462
Granite	Leuggern	2.52	2.66	2.60	0.02	984	0.8	7.5	3.4	1.3	984
	Böttstein	2.45	2.64	2.59	0.02	662	1.4	13.0	3.7	1.6	662
	GPK1	2.58	2.73	2.65	0.02	1005	0.7	5.9	1.8	0.8	1005
Leucogranite	GPK1	2.54	2.70	2.60	0.02	320	0.3	2.9	0.9	0.3	320
Monzonite	Schafisheim	2.58	2.90	2.79	0.05	456	6.5	16.1	9.8	1.8	456
Syenite	Schafisheim	2.61	2.94	2.80	0.07	532	3.2	20.5	10.4	2.9	532
Aplite	Schafisheim	2.55	2.66	2.61	0.02	242	1.2	2.8	1.8	0.4	242
	Leuggern	2.51	2.71	2.61	0.03	406	0.8	8.9	2.9	1.8	406
					Orthogneisses						
Gabbroic	Cajon	2.58	2.92	2.73	0.09	61	−0.1	9.6	2.7	2.2	61
Granodioritic	Cajon	2.31	2.79	2.58	0.09	720	−0.1	4.9	0.2	0.9	720
Dioritic	Cajon	2.30	2.91	2.68	0.10	1028	−0.2	8.3	1.6	1.4	1028
Granitic	Cajon	2.38	2.71	2.55	0.07	343	−1.3	2.4	0.5	0.5	343
	Moodus	2.59	2.70	2.62	0.01	298	−0.6	0.9	0.1	0.2	298
K-feldspar	Moodus	2.57	2.81	2.71	0.05	448	−0.6	4.3	2.1	1.0	448
Quartz–feldsp.	Moodus	2.53	2.85	2.68	0.07	264	−0.9	2.0	0.1	0.6	264
					Paragneisses						
(Sillimanite)	Leuggern*	2.49	2.81	2.68	0.04	903	3.6	19.6	8.0	2.5	903
Biotite gneiss	Leuggern†	2.50	2.81	2.7	0.04	1546	4.6	24.4	12.5	3.9	1546
	KTB-VB	2.40	2.92	2.74	0.04	1856	2.8	14.6	8.7	2.3	1856
	Moodus	2.68	2.82	2.76	0.02	755	1.4	5.8	3.2	0.8	755
Hornblende gneiss	Leuggern	2.47	2.85	2.72	0.06	130	0.9	19.7	6.0	4.5	130
	KTB-VB	2.68	3.01	2.86	0.05	664	6.1	15.9	11.1	1.5	664
	Moodus	2.54	2.95	2.73	0.06	1116	−0.6	5.6	1.1	0.9	1116
K-feldspar	KTB-VB	2.58	2.87	2.69	0.06	101	1.1	15.6	5.9	3.1	101
Quartz–plag.	KTB-VB	2.63	2.74	2.68	0.02	109	3.8	9.7	6.3	1.2	109

*Plagioclase–biotite gneiss (metagreywacke).
†Cordierite-bearing sillimanite–biotite gneiss (metapelite).

with granite density data from laboratory measurements (2.60 ± 0.07 g cm^{-3}; Landolt-Börnstein 1982). Monzonites and syenites are distinctly separated from the acid plutonics by higher-density values of 2.79 ± 0.05 g cm^{-3} and 2.80 ± 0.07 g cm^{-3}. Most of the gneissic rock types show broad value ranges, frequently skewed by very low-density values. This is particularly the case for the Cajon orthogneisses with density records lower than 2.45 g cm^{-3}. Although we restricted the data selection to intervals of good borehole conditions (caliper deviations $<10\%$ of bit size) and a general low tectonic overprint, low-density values were registered. They are explained as being related to small joints and fissures or borehole wall irregularities not detected prior to data analysis.

The P-wave velocity values of the selected rocks are between 3.2 km s^{-1} and 6.9 km s^{-1}. Mean values of the different rocks do not scatter significantly, and are between 5.1 ± 0.03 km s^{-1} and 6.1 ± 0.02 km s^{-1}. Surprisingly, P-wave velocity values are lower in the monzonites/syenites than in the granites/aplites, although the monzonites and syenites have higher density values. Values of the orthogneisses are high, with mean values of more than 5.8 ± 0.02 km s^{-1} and minimum values not below 5.0 km s^{-1}. Besides the hornblende gneisses, mean values of the paragneiss group are below 5.7 km s^{-1} and in a similar range to the plutonic rocks. Very low values (<4 km s^{-1}) are only observed for the Leuggern biotite gneisses and the KTB potassium-feldspar gneiss.

Beside the gamma-ray and the potassium log the neutron porosity exhibits the strongest differences between the rocks selected for this study. Most paragneisses are significantly separated from the orthogneisses, granites and aplites by their high neutron porosity values of up to almost 25%. Only the monzonites/syenites reach comparable value ranges. Granites,

Table 7. *Electrofacies statistics displayed for the different rock types. Minimum, maximum mean, and standard deviation of P-wave velocity and electrical resistivity data*

Lithology	Hole	Electrical resistivity (log ohm m)					P-wave velocity (km s^{-1})				
		Min	Max	Mean	SD	*n*	Min	Max	Mean	SD	*n*
					Plutonic rocks						
Biotite granite	Schafisheim	1.6	2.6	2.0	0.1	462	4.7	5.7	5.3	0.2	462
	Leuggern	2.4	4.8	3.9	0.7	984	4.9	5.9	5.6	0.2	984
	Böttstein	2.6	4.4	3.5	0.4	662	5.3	5.9	5.6	0.2	662
	GPK1	1.8	4.7	3.3	0.6	1005	5.3	6.3	5.8	0.2	1005
Leucogranite	GPK1	2.3	4.6	3.3	0.5	320	5.3	6.1	5.8	0.2	320
Monzonite	Schafisheim	1.3	3	2.1	0.4	456	4.9	5.9	5.5	0.2	456
Syenite	Schafisheim	1.8	1.4	2.9	0.2	532	4.4	5.9	5.4	0.2	532
Aplite	Schafisheim	2.6	3.9	3.3	0.2	242	5.2	6.0	5.7	0.1	242
	Leuggern	2.6	4.7	3.5	0.5	406	5.0	5.9	5.5	0.2	406
					Orthogneisses						
Gabbroic	Cajon	2.4	3.8	3.2	0.3	61	5.5	6.5	6.1	0.2	61
Granodioritic	Cajon	2.2	4.6	3.9	0.6	720	5.0	6.5	5.8	0.2	720
Dioritic	Cajon	2.0	4.6	3.5	0.6	1028	5.0	6.9	5.8	0.2	1028
Granitic	Cajon	2.8	4.6	4.5	0.3	343	5.2	6.4	5.9	0.2	343
	Moodus	3.0	4.6	4.2	0.2	298	5.6	6.4	5.9	0.2	298
K-feldspar	Moodus	3.3	4.0	3.8	0.1	448	5.2	6.0	5.6	0.1	448
Quartz–plag.	Moodus	2.9	4.8	3.8	0.4	264	5.7	6.4	6.1	0.2	264
					Paragneisses						
(Sillimanite)	Leuggern*	1.2	4.6	3.1	0.5	903	3.8	6.3	5.3	0.2	903
Biotite gneiss	Leuggern†	1.3	4.7	3.0	0.5	1546	3.2	6.0	5.1	0.3	1546
	KTB-VB	1.5	4.6	3.4	0.4	1856	4.8	6.2	5.6	0.2	1856
	Moodus	3.5	4.5	4.0	0.2	755	5.0	6.0	5.5	0.1	755
Hornblende	Leuggern	2.5	4.7	3.8	0.6	130	5.0	5.8	5.6	0.2	130
Gneiss	KTB-VB	1.7	4.9	3.6	0.5	664	5.6	6.6	6.1	0.2	664
	Moodus	2.8	5.0	4.0	0.4	1116	5.3	6.6	6.1	0.2	1116
K-feldspar	KTB-VB	2.3	3.4	2.9	0.4	101	3.9	5.8	5.4	0.3	101
Quartz–plag.	KTB-VB	2.3	3.8	3.4	0.3	109	5.5	5.8	5.7	0.1	109

*Plagioclase–biotite gneiss (metagreywacke).
†Cordierite-bearing sillimanite–biotite gneiss (metapelite).

aplites and orthogneisses generally do not exceed 10%. It is noticeable that the neutron porosity values of the Moodus borehole also show low values of less than 6% for the paragneisses.

Electrical resistivity values vary by several orders of magnitude, from 10^1 to 10^5 ohm m. They do not show any significant differences between the different rock types. In most cases mean resistivity values are above 10^3 ohm m, which is characteristic for massive igneous and crystalline rocks known from laboratory measurements (Landolt-Börnstein 1982). Significantly lower value ranges are observed for the Schafisheim granite, monzonite and syenites that point to borehole-specific influences, such as an overall higher microcrack density or stronger alteration.

Integrated analysis of log and rock data

The geochemical, petrographic and borehole geophysical data were compared in order to extract significant relationships between rock composition and log responses. This was performed using correlation analysis. Pearson correlation coefficients were calculated using the averages of logging, geochemical and mineralogical values of the different rock types. Besides the single mineral phases, correlation coefficients were also calculated for the mineral groups: (1) quartz, plagioclase and K-feldspar; (2) the total amount of biotite, muscovite, chlorite and amphibole; and (3) biotite, muscovite and K-feldspar. The results are given in Table 8. Results of correlation analysis between the log data and mineralogical and geochemical rock composition will be discussed and interpreted in the following sections.

Effects of rock mineralogy on log responses

The correlation between mineralogical rock data and wireline data reveals the following systematic observations.

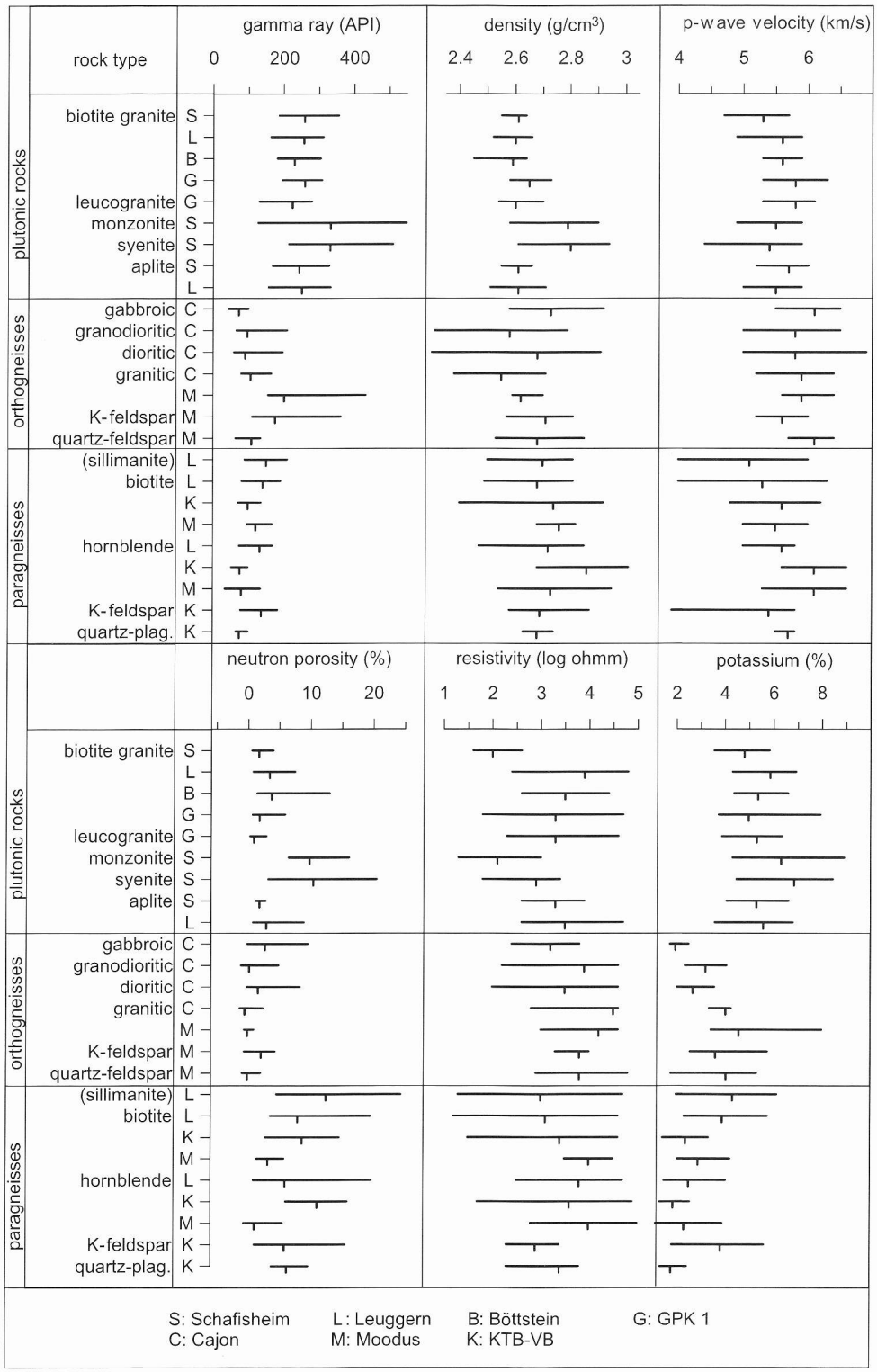

Fig. 4. Electrofacies of the different rock types. Displayed are minimum, mean and maximum values for the standard logs.

Table 8. *Pearson correlation coefficients calculated between mean values of geochemical, mineralogical and borehole geophysical data-sets*

Oxide/mineral	Gamma ray	Density	P-wave velocity	Neutron porosity	Potassium	Resistivity
SiO_2	−0.057	*−0.579	0.094	*−0.582	0.032	0.488
Al_2O_3	−0.282	−0.072	−0.139	0.307	−0.259	−0.105
K_2O	†0.807	−0.287	−0.315	−0.146	†0.874	−0.213
CaO	−0.201	*0.597	0.268	0.155	−0.278	−0.116
MgO	0.125	†0.709	0.102	0.410	0.060	−0.332
TiO_2	0.057	†0.762	−0.144	†0.665	−0.099	−0.417
Quartz	−0.304	−0.300	0.059	−0.265	−0.267	−0.496
K-feldspar	†0.634	−0.369	−0.092	−0.296	†0.697	−0.092
Plagioclase	*−0.591	−0.171	0.311	−0.315	*−0.568	0.239
Biotite	0.201	0.216	*−0.588	*0.500	0.239	−0.275
Muscovite	−0.172	0.117	−0.418	*0.510	−0.144	−0.119
Chlorite	−0.342	0.330	−0.012	0.406	−0.391	−0.108
Sillimanite	−0.044	0.049	−0.437	0.445	0.053	−0.159
Garnet	−0.117	0.109	−0.472	*0.610	−0.026	−0.152
Amphibole	−0.056	*0.546	0.286	0.254	−0.174	−0.245
Mica + Chl. + Amp.	−0.042	*0.619	−0.242	†0.704	−0.108	−0.401
Mica + K-feldspar	†0.746	−0.227	*−0.500	0.065	†0.825	−0.272
Quartz + K-feldspar + Plag	0.019	†−0.674	0.153	†−0.671	0.120	0.410

*Correlation is different from zero at a significance level of 0.05.
†Correlation is different from zero at a significance level of 0.01.

The most sensitive log for rock matrix variations for all gneisses and plutonic rocks is the gamma-ray log and, in particular, the potassium log, showing the highest correlation coefficients ($r > 0.8$) between rock and log data. Both parameters show comparable correlation coefficients with rock chemistry and mineralogy. Significant positive correlations are calculated between the K-feldspar content and the content of the mineral group K-feldspar plus biotite and muscovite. The relation to rock mineralogy is obvious, since K-feldspar, biotite and muscovite contain a considerable amount of potassium in their crystal lattice. Figure 5b shows the correlation between the potassium log and the total amount of K-feldspar plus biotite and muscovite. With regard to rock type and mineralogical composition (Table 2) the amount of K-bearing minerals controls the potassium and gamma-ray data to different degrees. In the acid orthogneisses, the rocks' potassium content is mainly related to the K-feldspars, while potassium content and gamma activity in the intermediate to basic gneisses is dependent on the amount of biotite.

The only significant negative correlation is calculated for the potassium, respectively the gamma ray versus the plagioclase content (Table 8). This can be explained by the substitution of K-feldspar by plagioclase in igneous rocks during magmatic differentiation, bearing in mind the rock classification after Streckeisen (1967).

Table 8 also reveals significant correlations between neutron porosity and rock composition. The highest positive correlation ($r = 0.7$) was calculated for the neutron log versus the amphibole plus biotite and muscovite content. Neutron porosity increases with the increasing amounts of these minerals (Fig. 5d). Rocks with high mica and amphibole contents, such as hornblende gneisses, biotite paragneisses, syenites and monzonites (see Table 2), plot in the upper right corner of Figure 5d, while granites, aplites and granitic rocks plot in the lower left-hand corner. In contrast, the neutron log is negatively correlated with the quartz plus K-feldspar and plagioclase content (Fig. 5c). Neutron porosity decreases with increasing amounts of quartz plus feldspar. In consequence, most granites, aplites and gneisses of granitic composition plot into the lower right edge of the cross-plot, while syenites/monzonites and most paragneisses have higher neutron and lower quartz/feldspar values. The high neutron-porosity values of some rock types and the observed correlation to rock mineralogy can be explained by the physical principles of the neutron-log measurement. Here, the hydrogen content is the most important factor controlling the neutron-log responses of a formation, since fast-emitted neutrons are slowed down predominantly by hydrogen nuclei occurring in the formation. Hydrogen can be kept in a formation in three different ways (Rider 1996):

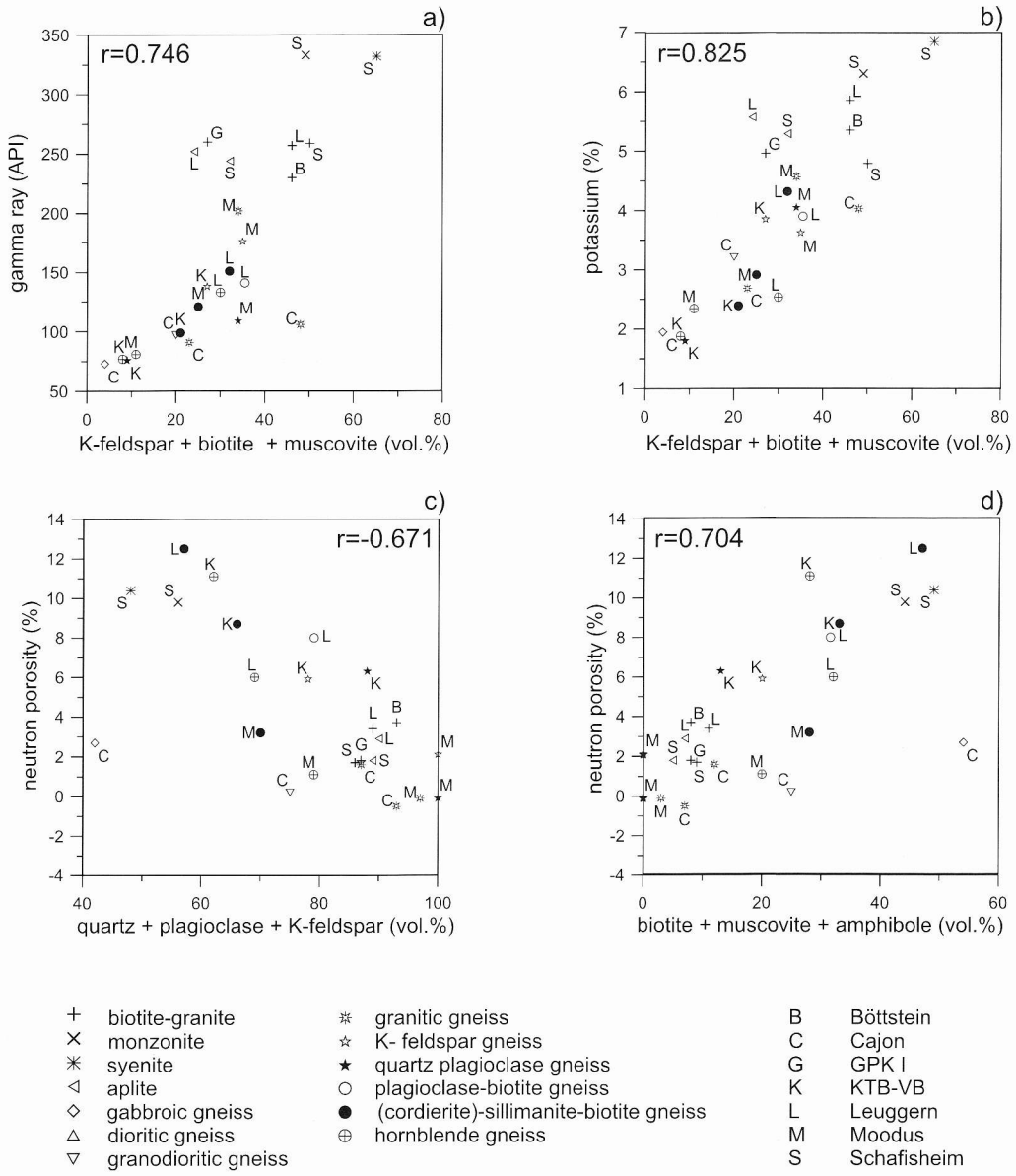

Fig. 5. Cross-plots of log responses of gamma ray, potassium, and neutron porosity, versus mineralogical composition of the rocks. Displayed are the average data from Tables 2 and 4. (**a**) & (**b**) Show positive trends between the gamma-ray/potassium logs with the total amount of micas and potassium feldspar within the rocks. (**c**) Shows the strong negative correlation between the neutron-porosity log and the quartz plus feldspar content. (**d**) Reveals the positive correlation between the neutron log and the total amount of OH-group bearing minerals. The corresponding Pearson correlation coefficients are given in Table 8.

(1) as free water in pores, fissures and fractures;
(2) as bound water incorporated within minerals; and
(3) as part of the crystal lattice in the form of OH-groups.

Since data selection was restricted to fresh, tectonically almost undisturbed crystalline rocks with effective porosities usually $<3\%$, the effect on the neutron log of free water in pores and fissures becomes negligible. This makes it evident that the recorded high neutron porosities in the crys-

talline rocks are not real in the sense of indicating rock porosity, but they are the result of rock matrix effects. Minerals with bound water are clay minerals such as montmorillonite and minerals of the zeolite group; however, neither occur in the investigated rocks. Therefore, only OH-bearing minerals can contribute significantly to the total hydrogen content in crystalline rocks. This fits with the results of Table 8, since amphibole and micas have OH-groups incorporated in their lattice and their concentration is positively correlated with the neutron log. On the contrary, quartz and feldspars are free of hydrogen and the occurrence of this mineral group is negatively correlated with neutron porosity.

There might be an argument that, besides the hydrogen in the formation, the atomic weight of the chemical elements also influences the (thermal) neutron log response (Schlumberger 1994), as there is a trend that elements with high atomic weights capture neutrons more effectively. Furthermore, the presence of certain rare-earth and trace elements with particularly large capture cross-sections (e.g. boron, lithium and cadmium) can have a significant effect on the neutron-log readings (Harvey *et al.* 1996). Rare-earth elements occur in acid/intermediate rocks, sometimes making quite a significant contribution. It can be assumed that the high neutron-log readings in crystalline rocks are produced by superposition of the different effects of hydrogen content, atomic weight and rare-earth element concentrations. Further investigations would be needed to separate the neutron-porosity readings for the different effects.

Correlation analysis has also revealed correlations between the density and rock mineralogy. A positive correlation ($r = 0.546$) is calculated for the relation between density and the amphibole content. A more significant negative correlation was calculated between density and the total amount of quartz and feldspar. The calculated results are explained by the different mineral densities, increasing from potassium feldspar (2.56 g cm^{-3}) to quartz (2.65 g cm^{-3}), to plagioclases (2.61–2.76 g cm^{-3}) and micas (2.7–3.1 g cm^{-3}), up to the mafic minerals of the amphibole group (3.15–1.25 g cm^{-3}) and the pyroxene group (2.9–3.5 g cm^{-3}) groups (Wohlenberg 1982; Schön 1996). Therefore, quartz/feldspar-rich rocks show low bulk density values, and mafic rocks with considerable amounts of amphibole/pyroxene have high rock densities.

Correlation analysis shows no significant correlations between P-wave velocity and mineral composition. A weak correlation was calculated only for the relationship between P-wave velocity and biotite and mica contents, respectively. These correlations are negative, indicating that average P-wave velocity decreases with mica content. At the moment there is no plausible explanation for this. In this study, correlation analysis reveals that the P-wave velocity log is not indicative of rock composition. However, it is known from laboratory measurements that rock-building minerals have characteristic P-wave velocities (Schön 1996) and that a relationship with rock modal composition does exist. Missing this relationship in our study could be explained by structural effects such as micro-cracks and foliation. Metamorphic rocks are characterized by pronounced foliation, which is known to influence the P-wave anisotropy considerably. In the KTB borehole, up to 15% P-wave anisotropy was measured within strongly foliated biotite gneisses, even under simulated *in situ* conditions (Berckhemer *et al.* 1997). The highest P-wave velocity values are measured parallel to foliation, while the lowest values are measured perpendicular to the foliation. Therefore, rock anisotropy could be an explanation for the strong scatter of *in situ* V_P data for the different rocks.

The resistivity log does not show any significant correlation with any of the main mineralogical components. This was expected, as the pore space of the selected crystalline rocks is very low and rock-forming minerals usually act as electrical isolators.

Effects of rock chemistry on log responses

The highest correlation coefficient ($r = 0.87$) between log data and rock chemical data is calculated between the potassium log and the K_2O content of the rocks (Table 8 & Fig. 6a). Small differences between the two types of data-set are caused by the principal differences in integration volume and sampling method between the continuous log data and the discrete core or cutting analyses. Taking into account the strong difference in the amount of data between core and log data, the high correlation between the two data sources is remarkable. Nevertheless, high potassium values in the log data may be biased, due to the calculation of potassium content from the total energy spectra of counted gamma-rays or by accumulation of potassium in the borehole mud. The latter was observed in mica-rich gneisses in the KTB-VB hole (Pechnig *et al.* 1997). Mica crystals became detached from the borehole wall and were kept in suspension in the mud. This caused gamma-ray log responses to increase by up to 10%.

A slightly smaller correlation coefficient ($r = 0.81$) was calculated for the gamma-ray and the K_2O content of the rocks. While the relation potassium log versus K_2O from cores represents variations in only one chemical element, the relation between gamma ray and versus K_2O from cores is also influenced by thorium and uranium. These two elements contribute to the total gamma-ray responses and thus change the gamma-ray/potassium ratio.

Significant correlations exist between the density log and the TiO_2 and MgO content. Titanium and magnesium have higher atomic weights than the other rock-forming elements

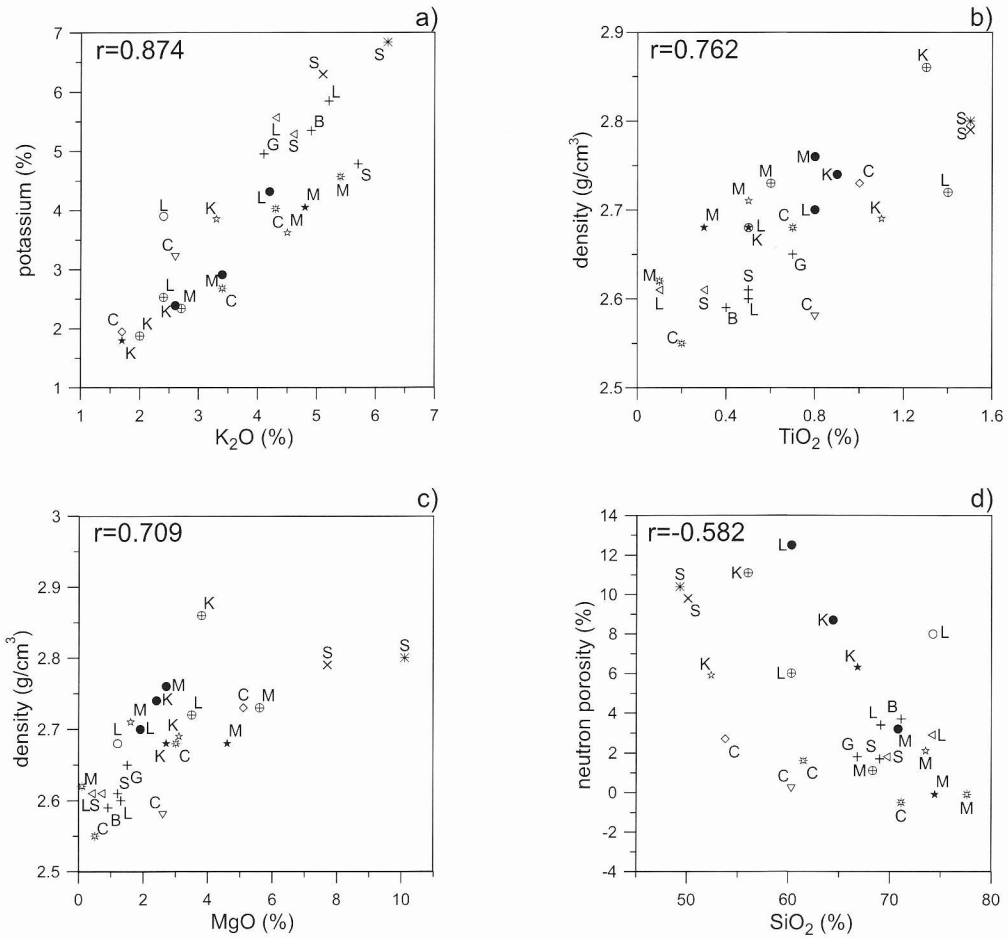

+	biotite-granite	✲	granitic gneiss	B	Böttstein
×	monzonite	☆	K-feldspar gneiss	C	Cajon
✳	syenite	★	quartz plagioclase gneiss	G	GPK I
◁	aplite	○	plagioclase-biotite gneiss	K	KTB-VB
◇	gabbroic gneiss	●	(cordierite)-sillimanite-biotite gneiss	L	Leuggern
△	dioritic gneiss	⊕	hornblende gneiss	M	Moodus
▽	granodioritic gneiss			S	Schafisheim

Fig. 6. Cross-plots of log responses of potassium, density, and neutron porosity versus the chemical composition of the rocks. Displayed are the average data from Tables 3 & 4. The corresponding Pearson correlation coefficients are given in Table 8.

silicon, aluminum, potassium and calcium, and they are preferentially incorporated into mafic minerals. High TiO_2 contents and high density values are therefore measured for the most mafic rocks: the Schafisheim monzonites/syenites, followed by the hornblende gneisses of Leuggern and KTB (Fig. 6b). The correlation between density and TiO_2 content is stronger than the one between density and MgO content. The latter is mainly caused by the very high MgO values of the monzonites and syenites, thus plotting separately from the general trend (Fig. 6c). A weak negative correlation ($r = -0.58$) occurs between density and SiO_2 content. A possible reason is a coupling of a decrease in mafic constituents with an increase in both quartz and feldspar.

The neutron porosity shows correlations comparable to those calculated between the density and the chemical elements. The highest coefficient is calculated for the relation between neutron porosity and the TiO_2 content. This might be due to different effects of:

(1) OH-groups incorporated in some mafic TiO_2-rich constituents;
(2) higher atomic weights of elements in mafic rocks; and
(3) the occurrence of trace elements.

The negative trend between the neutron porosity and the silicon content is also visible, although a strong scatter occurs between the data points.

The P-wave velocity and electrical resistivity logs show no significant correlation with any of the chemical elements. This is a further indication that these logging parameters are not significantly influenced by the chemical composition of the selected rocks.

Log correlation trends as result of mineralogical variability

Although significant correlations between log readings and rock composition exist, correlations between the log parameters are not detectable on

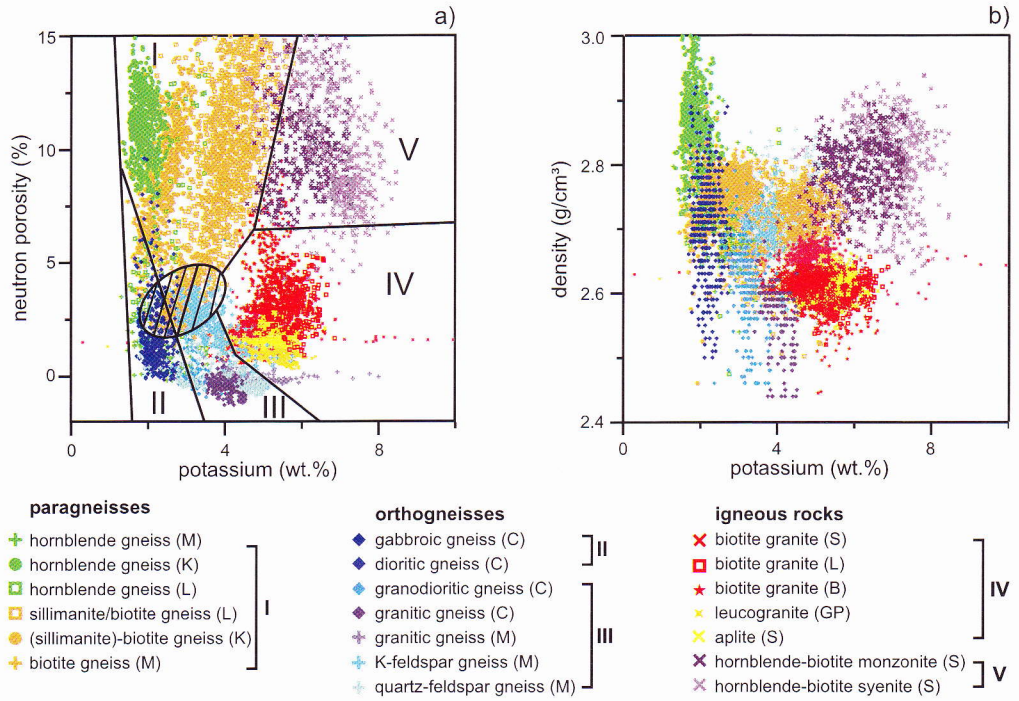

Fig. 7. Cross-plots of (**a**) potassium versus neutron porosity and (**b**) potassium log versus density, both showing the selected rock types. The potassium versus neutron porosity cross-plot makes it possible to span the classification fields to distinguish between the main rock groups: granites/aplites, monzonites/syenites, paragneisses, and acid to intermediate orthogneisses. Similar relationships between are also visible for the potassium–density cross-plot, but the separation of the groups is not as distinct as for the neutron–potassium plot. L, Leuggern; B, Böttstein; S, Schafisheim; GP, GPK1; C, Cajon Pass; M, Moodus; K, KTB.

the first viewing. When displayed as a cross-plot, the logging data show a large scatter (Fig. 7a & b). However, the cross-plot neutron porosity versus the potassium log allows the separation of the main rock types, since comparable rocks from different boreholes plot into the same plot areas (Fig. 7a). This is especially the case for the granites and aplites. More than 90% of these data plot between 0 and 7% neutron porosity and 4 and 7 wt% potassium. Also, the plot area of the orthogneisses is quite limited. The largest data scatter is produced by the paragneisses, especially for the neutron-porosity values, which range between 2% and >15%. The monzonites and syenites also exhibit a large data scatter. These rocks are clearly separated from the granite field and the paragneiss field. Significant overlaps between the main rock types exist between the paragneiss and the orthogneiss fields in the neutron porosity versus potassium plot. Rocks plotting in this area cannot be distinguished. Data clustering is also visible in the cross-plot density versus potassium, and the separation of the main rock types is not as sharp as in Figure 7a. This is especially the case for the orthogneisses, biotite paragneisses and hornblende gneisses, which show strong overlaps in the density field 2.6–2.8 g cm^{-3}. Granites and aplites are better separated by their high potassium values. This is also the case for the monzonites/syenites.

By separating the rocks into paragneisses and plutonic rocks, significant trends between log parameters become visible. The most prominent trends exist for the paragneisses, where two correlation trends occur. Within the large group of biotite gneisses, the gamma ray is positively correlated with the neutron porosity (Fig. 7) and the density log (Fig. 8). This correlation is clearly observed for all the biotite gneisses of the different boreholes, although offsets exist between the Leuggern and the Moodus/KTB data. The trends can be related to the rock mineralogical variability and will be explained by examples from the KTB biotite paragneiss. The mineralogical and chemical composition of this gneiss type varies considerably, with quartz concentrations ranging between 25% and 55%; biotite contents between 5% and 40%; and muscovite contents between 3% and 38% (Table 2). The varying quartz–mica ratios are reflected in the chemical composition: i.e. SiO_2 values between 45% and 75% and K_2O contents between 2.2% and 3.6% (Table 3). Petrographic studies revealed two end-members of the KTB biotite gneisses: a quartz-rich type with high SiO_2 values, and a mica-rich rich variety with increased potassium contents (Müller *et al.* 1989). By comparing

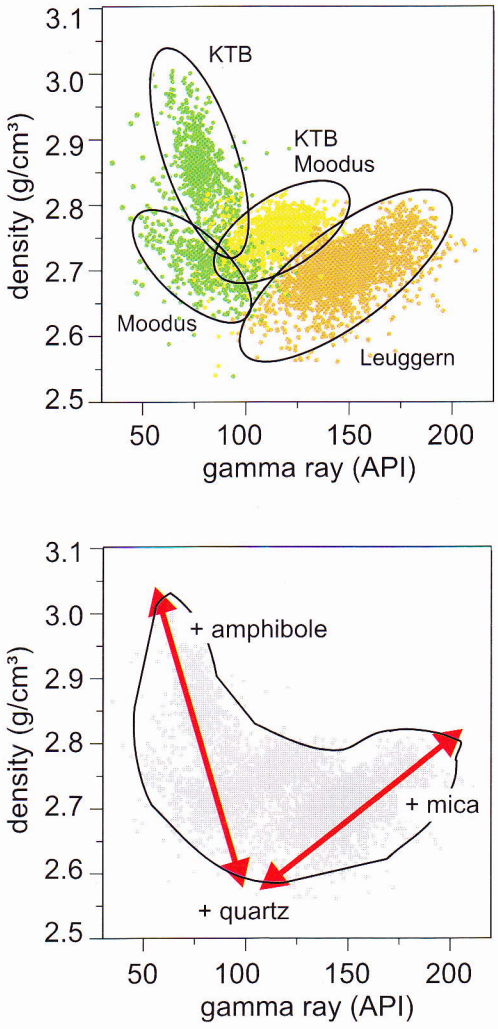

Fig. 8. Diagram of the mineralogical end-members controlling the relationship between the density and gamma array in paragneisses. For signatures, see Figure 7.

mineralogical and chemical data with logging data it was demonstrated (Haverkamp & Wohlenberg 1991; Pechnig *et al.* 1997) that the mica-rich paragneisses have much higher gamma-ray, potassium, density and neutron-porosity values than the quartz-rich types. This can be explained by mineral physics and chemistry. Micas are the most important potassium-bearing minerals in the biotite paragneisses, and thus they contribute significantly to the measured total gamma activity. Micas have higher densities than quartz (muscovite: 2.83 g cm^{-3}, biotite: 3.01 g cm^{-3}, quartz: 2.65 g cm^{-3}), and they

have incorporated OH-groups in their lattice. After Serra (1986) a rock consisting of 100% of mica would produce 20–25% apparent porosity in the neutron-log readings, while pure quartz would produce a neutron-log response of −2%.

The relationship between the quartz/mica ratio and the logging data exists also for the Leuggern and Moodus gneisses. In all boreholes, the end-members of the observed trends are, as marked by the arrows in Figure 8, quartz-rich gneisses with low density and low gamma-ray values on the one hand, and mica-rich gneisses with high density and high gamma-ray values on the other hand. In particular, the Leuggern biotite gneisses show a pronounced modal variability. Quartz contents vary between 15% and 50%, and total mica plus sillimanite content can be more than 60% (Table 2). This produces total gamma-ray values varying from 80 to more than 200 API (Table 5a), and log density ranging between 2.49 and 2.81 g cm^{-3}.

The hornblende gneisses of the Moodus and the KTB borehole show divergent trends. In contrast to the biotite gneisses, density and gamma ray are negatively correlated (Fig. 8). The main components of hornblende gneisses are quartz, feldspar, biotite and amphibole, in variable amounts (Table 2). Gneisses with low amphibole contents have high quartz contents of, and vice versa. Enrichment in quartz corresponds with the change to a more acid geochemical composition of the rocks, which is also accompanied by a potassium increase. Since amphiboles have a significant higher density than quartz, the compositional changes produce a trend with the following end-members: amphibole-rich hornblende gneisses with low gamma-ray values and high density values on the one hand, and quartz- and plagioclase-rich hornblende gneisses with low densities on the other (Fig. 8).

Plotting data from the orthogneisses and plutonic rocks in the cross-plot density versus potassium does not reveal significant trends (Fig. 9) as observed for the paragneisses. A negative correlation between density and potassium is visible for the orthogneisses, which can be explained by mineralogical variations similar to those of the hornblende gneisses. Mineralogical end-members of this trend are biotite–amphibole-rich orthogneisses of gabbroic/dioritic composition with the highest densities, and quartz–plagioclase-rich orthogneisses of granodioritic/granitic composition with the lowest densities. Gamma activity and potassium values increase significantly in the field of granites and aplites. Here, only a weak trend is visible. This trend is caused by the enrichment of K-feldspar in these rocks. Due to the substitution of K-feldspar and plagioclase in granites,

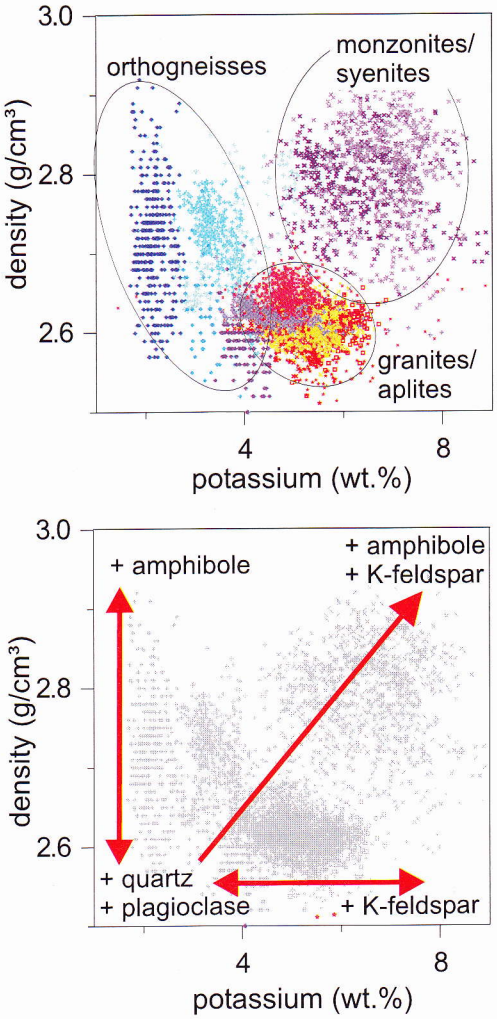

Fig. 9. Diagram of the mineralogical end-members controlling the relation between the density and the potassium log in orthogneisses and plutonic rocks. For signatures, see Figure 7.

potassium values vary over a considerable range. Since the density of K-feldspar, plagioclase and quartz (the main components of the granites and aplites, Table 2), is more or less the same, rock density is not affected by the mineralogical variability.

The monzonites and syenites are separated from the granites and orthogneisses, and show a data scatter without any trends visible. These rocks exhibit high variability in the potassium and density values, which is related to the changing amounts of their components. High density and high potassium values in syenites/

monzonites are related to the enrichment of both minerals, hornblende and potassium feldspar.

In summary, for the orthogneisses and plutonic rocks, the relation between the density and potassium log is controlled by the relative amount of the mineral assemblages: amphibole plus biotite, quartz plus plagioclase, and potassium feldspar.

Conclusions

Mineralogical, geochemical and *in situ* petrophysical data-sets were compiled for this study in order to explain log responses in relation to rock composition for acid to intermediate gneisses and plutonic rock. Correlation analysis between the different data types reveals significant correlations between some of the standard logs and rock mineralogy. The most prominent are the gamma-ray and potassium logs as indicators for the potassium feldspar and mica content. In addition, the density and neutron-porosity log are indicative of the rock composition. They are strongly controlled by the relative amount of amphibole plus mica versus quartz plus feldspar. P-wave velocity and electrical resistivity are essentially independent of rock composition.

These results show that in the investigated rock types the standard logging parameters are of a different importance for lithology prediction. Density-log and neutron-porosity devices, which are used in the sedimentary environment as porosity predictors, are indicative of mineralogical changes in the crystalline environment. The most powerful discrimination between different rock types is given by a combination of the gamma-ray and the potassium logs on the one hand versus the neutron and density logs on the other. The combination of neutron versus potassium logs is suitable for discriminating between the main rock types.

Strong correlations between logging parameters are also observed within the major rock groups. Integration of petrophysical log data with information on rock composition reveals three major mineralogical background parameters which are controlling the log responses in gneisses and acid to intermediate plutonic rocks. In paragneisses, log correlations follow the ratios of the amphibole, quartz and mica. In the orthogneisses and granites/aplites this is biotite plus amphibole versus K-feldspar plus quartz, following the magmatic differentiation from mafic to acid rocks. Syenites and monzonites strongly separate from this trend, since potassium feldspar occurs together with amphibole and biotite.

This study used logging data and core data from various boreholes, collected and composed from different sources. The German Continental Drilling Project (KTB) was funded by the German Ministry of Research and Technology (BMFT). KTB data were made available by the GeoForschungszentrum (GFZ) Potsdam, Germany. Logging data from the Leuggern, Böttstein and Schafisheim boreholes were kindly made available by NAGRA (National Co-operative for the Disposal of Radioactive Waste). Data from the borehole GPK1 Soultz-sous-Forêts were made available by the Bureau de recherches géologiques et minières, and the digital logging data-sets of the Moodus and Cajon Pass borehole were kindly provided by the Borehole Research Group of the Lamont–Doherty Earth Observatory, NY, USA. Parts of this study were funded by the German Science Foundation (DFG, Wo-159/11; Wo-159/14). We would also like to thank Prof. J. Wohlenberg for initiating these studies and for making them possible.

References

ADAMS, J. A. S., OSMOND, J. K. & ROGERS, J. J. W. 1959. The geochemistry of thorium and uranium. *In*: AHRENS, L. H., PRESS, F., RANKAMA, K. & RUNCORN, S. K. (eds) *Physics and Chemistry of the Earth*, **3**, 298–348.

AMBERS, C. P. 1989. *Core and Cuttings Descriptions of the 1987 Moodus 4764 Foot Deep Well*, Connecticut. Connecticut Geological and Natural History Survey, Open File Report **89-1**, 207 pp.

BERCKHEMER, H., RAUEN, A. *et al.* 1997. Petrophysical properties of the 9-km-deep crustal section at KTB. *Journal of Geophysical Research*, **102**, 18 337–18 361.

CHEVREMONT, P. & GENTER, A. 1989. *Etude Pétrologique des Échantillons de Granite de Soultz-sous-Forêts, Forage GPK1*. Note interne 89/IRG, 20.

DANIELS, J. J., SCOTT, J. H., & OLHOEFT, G. R. 1993. Interpretation of core and well log physical property data from drill hole UPH-3, Stephenson County, Illinois. *Journal of Geophysical Research*, **88**, 7346–7354.

DESBRANDES, R. 1982. *Encyclopedia of Well Logging*, Edition Technips, Paris, 548 pp.

ELLIS, D. V. 1987. *Well Logging for Earth Scientists*. Elsevier, Amsterdam, 532 pp.

EMMERMANN, R. & LAUTERJUNG, J. 1997. The German Continental Deep Drilling Program KTB: overview and major results. *Journal of Geophysical Research*, **102**, 18 179–18 201.

GENTER, A. 1989. *Géothermie Roches Chaudes Sèches: le granite de Soultz-sous-Fôrets (Bas-Rhine, France). Fracturation naturelle, altération hydrothermale et interaction eau–roche*. Thèse de doctorat de l'Université d'Orléans, France, 201 pp.

GENTER, A., BEAUFORT, A., MEUNIER, A. & CHEVREMONT, P. 1989. Etude des altérations hydrothermales du granite de Soultz-sous-Fôrets–Forage GPK1. *Rapport BRGM 89*, SGN 295 EEE/IRG.

HARVEY, P. K., LOVELL, M. A., BREWER, T. S., LOCKE, J. & MANSLEY, E. 1996. Measurements of thermal neutron absorption cross section in

selected geothermal reference material. *Geostandard Newsletter*, **20**, 79–85.

HAVERKAMP, S. & WOHLENBERG, J. 1991. EFA-Log-Rekonstruktion kristalliner Lithologie anhand von bohrlochgeophysikalischen Messungen für die Bohrungen URACH 3 und KTB-Oberpfalz VB. *KTB Report*, **91-4**, 213 pp.

HEARST, J. R., NELSON, P. H. & PAILLET, F. L. 2000. *Well Logging for Physical Properties. A Handbook for Geophysicists, Geologists and Engineers*, 2nd edn, Wiley, Chichester, UK.

HEINSCHILD. H. J., HOMANN, K., STROH, A. & TAPFER, M. 1988. Tiefbohrung KTB Oberpfalz VB, Ergebnisse der geowissenschaftlichen Bohrungsbearbeitung im KTB Feldlabor, Teufenbereich 480 bis 992 m: C. Geochemie. *In*: EMMERMANN, R., DIETRICH, H. G., HEINISCH, M. & WÖHRL, T. (eds) *KTB-Report*, **88-2**, C1–C107, Hannover, Germany.

HIRSCHMANN, G, DUYSTER, J., HARMS, U., KOTNY, A., LAPP, M., DE WALL, H., ZULAUF, G. 1997. The KTB superdeep borehole: petrography and structure of a 9-km-deep crustal section. *Geologische Rundschau*, **86**, 3–14.

KEYS, W. S. 1979. Borehole geophysics in igneous and metamorphic rocks. *Transactions, SPWLA, 20th Annual Logging Symposium*, Tulsa, Oklahoma, paper OO.

LACHENBRUCH, A. H. & SASS, J. H. 1988. The stress heat-flow paradox and thermal results from Cajon Pass. *Geophysical Research Letters*, **15**, 981–984.

LANDOLT-BÖRNSTEIN 1982. Zahlenwerte und Funktionen aus Naturwissenschaften und Technik. *Neue Serie Vol. 1: Physical Properties of Rocks*, Subvol. b. – 604 S., Springer, Berlin, Heidelberg and New York.

MATTER, A., PETERS, T., BLÄSI, H., SCHENKER, F. & WEISS, H. P. 1988. Sondierbohrung Schafisheim – Geologie; Text- und Beilagenband. *Nagra Technische Berichte NTB 86-03*, Nagra, Wettingen, Switzerland.

NAUMHOFF, P. 1988. Lithology and structure identified in a 1.5 km borehole near Moodus, Connecticut. *EOS*, **69**, p. 491.

NELSON, P. H. & JOHNSTON, D. 1994. Geophysical and geochemical logs from a copper oxide deposit, Santa Cruz Project, Casa Grande, Arizona. *Geophysics*, **59** (12), 1827–1838.

O'BRIEN, P. J., DUYSTER, J., GRAUERT, B., SCHREYER, W., STÖCKHERT, B. & WEBER, K. 1997. Crustal evolution of the KTB drill site: from oldest relics to the late Hercynian granites. *Journal Geophysical Research*, **102**, 18 203–18 220.

PECHNIG, R., HAVERKAMP, S., WOHLENBERG, J., ZIMMERMANN, G. & BURCKHARDT, H. 1997. Integrated log interpretation in the German Continental Deep Drilling Program: lithology, porosity, and fracture zones. *Journal Geophysical Research*, **102**, 18 363–18 390.

PETERS, T. J., MATTER, A., BLÄSLI, H.-R. & GAUTSCHI, A. 1986. Sondierbohrung Böttstein – Geologie; Text- und Beilagenband, *Nagra Techn. Ber. NTB 85-02*, Nagra, Wettingen, Switzerland.

PETERS, T. J., MATTER, A., BLÄSLI, H.-R., ISENSCHMID, CH., KLEBOTH, P., MEYER, CH. & MEYER, J. 1989*a*. Sondierbohrung Leuggern – Geologie; Text- und Beilagenband, *Nagra Techn. Ber. NTB 86-05*, Nagra, Wettingen, Switzerland.

PETERS, T. J., MATTER, MEYER, J., ISENSCHMID, CH. & ZIEGLER, H.-J. 1989*b*. Sondierbohrung Kaisten – Geologie; Text- und Beilagenband, *Nagra Techn. Ber. NTB 86-04*, Nagra, Wettingen, Switzerland.

PRATSON, E. L., ANDERSON, R. N., DOVE, R. E., LYLE, M., SILVER, L. T., JAMES, E. J. & CHAPPELL, B. W. 1992. Geochemical logging in the Cajon Pass drill hole and a new, oxide, igneous rock classification scheme. *Journal Geophysical Research*, **97**, 5167–5180.

RIDER, M. 1996. *The Geological Interpretation of Well Logs*. Whittles Publishing, Caithness, Scotland, UK, 280 pp.

ROGERS, J. J. W. & ADAMS, J. A. S. 1969*a*. Thorium. *In*: WEDEPOHL, K. H. (eds) *Handbook of Geochemistry*, **2** (4), 90B–90O, Springer, Berlin.

ROGERS, J. J. W. & ADAMS, J. A. S. 1969*b*. Uranium. *In*: WEDEPOHL, K. H. (eds). *Handbook of Geochemistry*, **2** (4), 92B–92O, Springer, Berlin.

SATTEL, G. 1986. FACIOLOG – Anwendung eines Programmsystems zur Charakterisierung der Kristallin-Lithologie. *Nagra Informiert*, **1**, 18–24.

SCHLUMBERGER 1994. Neutron porosity logging revisited. *Oilfield Review*, October, 4–8.

SCHÖN, J. H. 1996. Physical properties of rocks – fundamentals and principles of petrophysics. HELBIG, K. & TREITEL, S. (eds) *Handbook of Geophysical Exploration, Section I, Seismic Exploration*, Vol. 18. Pergamon, Oxford, 583 pp.

SERRA, O. 1984. *Fundamentals of Well-Log Interpretation*. Vol. 1, Elsevier, Amsterdam.

SERRA, O. 1986. *Fundamentals of Well-Log Interpretation*. Vol. 2, Elsevier, Amsterdam.

SILVER, L. T., JAMES, E. W. & CHAPPELL, B. W. 1988. Petrological and geochemical investigations at the Cajon Pass Deep Drillhole. *Geophysical Research Letters*, **15**, 961–964.

STRECKEISEN, A. 1967. Classification and nomenclature of igneous rocks. *Neues Jahrbuch Mineralogische Abhandluagen*, **107**, 144–214.

STROH, A. & TAPFER, M. 1988. Tiefbohrung KTB Oberpfalz VB, Ergebnisse der geowissenschaftlichen Bohrungsbearbeitung im KTB Feldlabor, Teufenbereich 0–480 m: C. Geochemie. *In*: EMMERMANN, R., DIETRICH, H. G., HEINISCH, M. & WÖHRL, T. (eds) *KTB-Report*, **88-1**, C1–C73, Hannover.

TAPFER, M., HEINSCHILD. H. J., STROH, A., WITTENBECHER, M. & ZIMMER, M. 1989. Tiefbohrung KTB Oberpfalz VB, Ergebnisse der geowissenschaftlichen Bohrungsbearbeitung im KTB Feldlabor, Teufenbereich 2500–3009,7 m: C. Geochemie. *In*: EMMERMANN, R., DIETRICH, H. G., HEINISCH, M. & WÖHRL, T. (eds) *KTB-Report*, **89-4**, C1–C50, Hannover.

THURY, M., GAUTSCHI, A. *et al.* 1994. Geology and hydrology of the crystalline basement of northern Switzerland. *Geologische Berichte Nr.*

18, Bundesamt für Umwelt, Wald und Landschaft, Bern, Switzerland.

TRAINEAU, H. A., GENTER, J. P., CAUTRU, F., FABRIOL, H. & CHEVREMONT, P. 1992. Petrography of the granite massif from drill cutting analysis and well log interpretation in the geothermal HDR borehole GPK1 (Soultz, Alsace, France). *In*: BRESEE, J.C. (eds). *Geothermal Energy in Europe*, 1–29, Gordon and Breach Science Publishers, Switzerland.

VINCENT, M. W. & EHLIG, P. L. 1988. Laumontite mineralization in rocks exposed of San Andreas Fault at Cajon Pass, Southern California. *Geophysical Research Letters*, **15**, 977–980.

WILSON, M. 1989. *Igneous Petrogenesis.* Unwin Hyman, London.

WINTSCH, R. P. & ALEINIKOFF, J. N. 1987. U–Pb Isotopic and geological evidence for Late Paleozoic anatexis, deformation, and accretion of the Late Proterozoic Avalon Terrane. *American Journal of Science*, **287**, 107–126.

WITTENBECHER, M., HEINSCHILD, H. J., STROH, A. & TAPFER, M. 1989. Tiefbohrung KTB Oberpfalz VB, Ergebnisse der geowissenschaftlichen Bohrungsbearbeitung im KTB Feldlabor, Teufenbereich 3009, 7–3500 m: C. Geochemie. *In*: EMMERMANN, R., DIETRICH, H. G., HEINISCH, M. & WÖHRL, T. (eds) *KTB-Report*, **89-5**, C1–C62, Hannover, Germany.

WOHLENBERG, J. 1982. Dichte der Minerale und Gesteine. *In*: ANGENHEISTER, G. (eds) *Landolt Börnstein – Physikalische Eigenschaften der Gesteine.* Subvolume A, 66–119, Springer, Berlin, Heidelberg and New York.